

# Greenland's contribution to global sea-level rise by the end of the 21st century

Rune G. Graversen · Sybren Drijfhout ·  
Wilco Hazeleger · Roderik van de Wal ·  
Richard Bintanja · Michiel Helsen

Received: 4 May 2010 / Accepted: 19 September 2010  
© Springer-Verlag 2010

**Abstract** The Greenland ice sheet holds enough water to raise the global sea level with  $\sim 7$  m. Over the last few decades, observations manifest a substantial increase of the mass loss of this ice sheet. Both enhanced melting and increase of the dynamical discharge, associated with calving at the outlet-glacier fronts, are contributing to the mass imbalance. Using a dynamical and thermodynamical ice-sheet model, and taking into account speed up of outlet glaciers, we estimate Greenland's contribution to the 21st-century global sea-level rise and the uncertainty of this estimate. Boundary fields of temperature and precipitation extracted from coupled climate-model projections used for the IPCC Fourth Assessment Report, are applied to the ice-sheet model. We implement a simple parameterization for increased flow of outlet glaciers, which decreases the bias of the modeled present-day surface height. It also allows for taking into account the observed recent increase in dynamical discharge, and it can be used for future projections associated with outlet-glacier speed up. Greenland contributes 0–17 cm to global sea-level rise by the end of the 21st century. This range includes the uncertainties in climate-model projections, the uncertainty associated with scenarios of greenhouse-gas emissions, as well as the

uncertainties in future outlet-glacier discharge. In addition, the range takes into account the uncertainty of the ice-sheet model and its boundary fields.

**Keywords** Sea-level-rise projection · Greenland ice sheet · Outlet glacier · Ice-sheet modeling

## 1 Introduction

The Earth's two major ice sheets, the Antarctic and the Greenland ice sheet, hold enough water to raise the sea-level by around 64 m (Bamber et al. 2001; Lythe et al. 2001). Climate-model projections suggest that temperature and precipitation increase over both ice sheets during 21st century (Meehl et al. 2007a). Since melt temperatures in summer are reached over large parts of the Greenland ice sheet, especially along its margin, the mass loss associated with raising temperatures is expected to more than offset the mass gain due to the increase of precipitation (Gregory and Huybrechts 2006). In Antarctica, in contrast, the precipitation is expected to be the dominating term, because summer temperatures are in general well below the freezing point—even by the end of the 21st century—except in the Peninsula region.

The total mass balance of the ice sheets is determined by precipitation, melting and calving at the ice front. Accumulation from precipitation, and ablation from melting constitute the surface mass balance (SMB), whereas calving is often referred to as dynamical discharge. The International Panel of Climate Change (IPCC) Fourth Assessment Report (AR4) projects that the SMB of the two ice sheets will change during the years ahead. This results in a 1–12 cm sea-level-rise contribution from Greenland by the end of the 21st century relative to 1990, which is

---

R. G. Graversen (✉)  
Royal Netherlands Meteorological Institute,  
Wilhelminalaan 10, 3732 De Bilt, The Netherlands  
e-mail: graversen@knmi.nl; rune@misu.su.se

S. Drijfhout · W. Hazeleger · R. Bintanja  
Royal Netherlands Meteorological Institute,  
De Bilt, The Netherlands

R. van de Wal · M. Helsen  
Institute for Marine and Atmospheric Research Utrecht,  
Utrecht University, Utrecht, The Netherlands

compensated by a negative contribution from Antarctica of 1–14 cm. These estimates are based on temperature projections by various state-of-the-art climate models assuming a simple relation between global temperature change and the SMB. This temperature-SMB relation is based on a study with high-resolution climate models (Gregory and Huybrechts 2006). The sea-level-change ranges reflect uncertainty in temperature projections due to various greenhouse-gas emission scenarios (Nakićenović and Swart 2000), as well as spread among climate models. They also include uncertainty of the temperature-SMB relation and of the SMB calculation itself (Gregory and Huybrechts 2006).

Although the SMB for the Antarctic ice sheet is positive during the 21st century, according to the AR4, the ice sheet may still be shrinking over this period due to an increase of dynamical discharge. The major part of the ice loss in Antarctica is caused by dynamical discharge associated with calving. Changes in the dynamical discharge are hard to predict, can occur suddenly, and may be substantial (Meehl et al. 2007a). The AR4 projects that a change in the dynamical discharge from both ice sheets adds  $-0.4$  to  $7.4$  cm to the sea level. This estimate is based on extrapolating into the future the observed increase in dynamical discharge from the two ice sheets during 1993–2003. It is assumed that this discharge includes the total mass-loss increase from Antarctica plus half of that from Greenland (the other half of the mass loss from Greenland is attributed to the change of the SMB). In addition, the AR4 projects a small sea-level-rise contribution from dynamical changes of the ice sheet, which can be simulated with ice-sheet models, and which is assumed to be no more than 10% of the SMB. This is estimated by comparing mass loss associated with a given SMB in model experiments where the topography was fixed with experiments where it was free to vary. Finally, the AR4 presents two additional dynamical discharge scenarios, where the increase over 1993–2003 is either assumed to saturate exponentially or increase with global-mean temperature. These projections add between  $-1$  and  $17$  cm to 21st century sea-level rise.

With the present work, we intent to provide a better estimate of the range of uncertainty of the 21st-century sea-level-rise contribution from the Greenland ice sheet. Ice-sheet flow models are forced directly with climate-model projections of temperature and precipitation over Greenland as an alternative to the more simple method based on a relation between sea-level and global temperature used for the AR4. We use an ensemble of ice-sheet models that differ by the settings of parameters and scaling of boundary fields within their ranges of uncertainties. This leads to an estimate of the ice-sheet model uncertainty, which is the uncertainty in the sea-level response for a given scenario of temperature and precipitation changes. We also implement

a more advanced way for projection of sea-level change associated with an increase of the dynamical discharge than that used for the AR4.

Greenland has a myriad of fjords, some of them cutting into the present-day ice sheet. Most of them are less than 5 km wide and are therefore not resolved on today's ice-model grids which have a resolution normally between 5 and 20 km. At the fjords, the ice may flow fast since the bottom friction is considerably smaller than under the surrounding ice (Joughin et al. 2004). Hence these fjords constitute corridors where the ice is transported away from the bulk of the ice sheet. Such dynamical discharge of the ice sheet is only to a limited extent reproduced by the ice-sheet models, partly due to the low model resolution compared to the scales of the fjords, and partly due to the approximations applied for the dynamical part of the models.

Here we mimic the effect of outlet glaciers by increasing the sliding at the model grid-points in the vicinity of fjords. This parameterization also allows for taking into account the recently observed enhancement of outlet-glacier flow (Joughin et al. 2004; Rignot et al. 2008; Howat et al. 2008). In addition, the parameterization can be used for predictions of the outlet-glacier contribution to future sea-level rise, as an alternative to the simple extrapolation method used for the AR4.

An increase of sea-surface temperatures in the vicinity of Greenland fjords has been reported, which may contribute to melt and speed-up of outlet glaciers (Holland et al. 2008; Straneo et al. 2010). Although we do not model this process, its effect on outlet glaciers is expected to be included by the outlet-glacier parameterization.

## 2 Model and experiment description

Greenland's contribution to the 21st century sea-level rise is estimated by using an ice-sheet model forced with climate-model projections of temperature and precipitation over Greenland.

### 2.1 Ice-sheet model

The ice-sheet model provides prognostic estimates of the ice-sheet thickness,  $H$ , on the basis of the mass continuity equation:

$$\frac{\partial H}{\partial t} = -\nabla \cdot (\mathbf{v}H) + M - D,$$

where  $M = A - R$  is the surface-mass balance which is equal to accumulation,  $A$ , from snow and, to some extent, rain, minus runoff,  $R$ . Dynamical discharge associated with calving at the ice front is indicated by  $D$ . It is assumed that whenever ice is no longer grounded and starts floating, it

breaks off, which constitutes  $D \cdot \mathbf{v}$  is the vertically averaged ice velocity,  $t$  is time, and  $\nabla = (\frac{\partial}{\partial x}, \frac{\partial}{\partial y})$  is the horizontal divergence operator. This equation states that the ice-thickness tendency at any grid point is determined by the sum of a divergence and source/sink terms. The ice-sheet-model system includes a dynamical model for the divergence term, and a mass-balance model for the  $M$  term. In addition it includes a bed-rock-adjusting model (e.g. Huybrechts and de Wolde 1999). All these models are coupled and constitute together what we refer to as the ice-sheet model. This ice-sheet model has been used previously in a number of earlier studies (Van de Wal 1999a; Van de Wal 1999b; Bintanja et al. 2002; Bintanja et al. 2005; van den Berg et al. 2008; Bintanja and van de Wal 2008).

### 2.1.1 Dynamical model

The dynamical part of the ice-sheet model is based on the zero-order shallow-ice approximation for a force balance of stress variations, and the empirical Glen's flow law for the viscosity (e.g. Huybrechts 1990). All forces acting on a segment of the ice sheet are assumed to be in balance, which implies that the ice velocities can be diagnostically estimated. The viscosity depends on the ice temperatures which are estimated prognostically by solving the thermodynamic equation on the basis of three-dimensional ice advection, diffusion, friction, geothermal heat flux at the bottom, and annual-mean surface-air temperatures at the top. The viscosity tensor is also dependent on the vertical variations of the anisotropy of ice, which is taken into account by varying a flow enhancement factor with depth following Mangeney and Califano (1998). Sliding at the bottom occurs when the temperature in the lowest ice level reaches the pressure-melting point following Huybrechts (1990). The model has a 10 x 10 km horizontal resolution and 15 height levels.

For fast ice streams, having sliding at the bottom, the horizontal deviatoric stresses may become important, hereby violating the zero-order shallow-ice approximation (Hindmarsh 2006). First attempts are made to take the dynamics of these fast ice streams into account (e.g. Bueler and Brown 2009), but these models are still in the testing phase.

### 2.1.2 Mass-balance model

Accumulation and ablation are estimated on the basis of the annual precipitation and the annual cycle of surface-air temperatures, using a positive degree-days (PDD) approach at each model grid point (Reeh 1991). The annual temperature cycle is approximated by a sinus curve with the amplitude given from the difference between the July and the annual-mean temperatures. The diurnal cycle and daily

variability are taken into account by adding to the annual cycle a Gaussian temperature distribution with a standard deviation of around 5°, following Reeh (1991). The surface-air temperatures are parameterized on the basis of height and latitude (Ohmura 1987; Huybrechts and de Wolde 1999): Both the July and annual-mean temperatures decrease linearly with latitude and height. At low altitude in the north, the annual-mean temperature is set up to 3.2°C colder than given by this linear relation in order to take the frequent occurrence of surface inversions into account.

The precipitation is averaged over the period 1990–2008 and is based on an estimation by RACMO (Ettema et al. 2009), a high-resolution (~11 km and 40 hybrid levels) regional climate model, driven with ERA-40 reanalysis data (Uppala et al. 2005) for the period up to September 2002, and operational analysis data thereafter; both these data sets are from the European Centre for Medium-Range Weather forecasts (ECMWF).

For a given calendar day, first snow and then ice will melt if positive temperature conditions, quantified as a PDD potential, appear. Following Pfeffer et al. (1991), rain and water from snow-melt will partly seep into the underlying snow and refreeze during winter if snow is still present after the melt season. Precipitation is assumed to fall as rain when temperatures exceed 1°C.

## 2.2 Experimental design

The ice-sheet models are applied with boundary fields, such as temperature, precipitation, and sea level, both for the past, present-day, and the future. Figure 1 provides an overview of the application of these fields.

### 2.2.1 The last glacial cycle

Due to slow ice movements and low thermal conductivity, the ice temperatures in the interior of the large ice sheets, have a memory of past climates on the time scales of multiple millennia. Since the temperature of the ice is important for its viscosity and hence for its flow, we initialize the ice-sheet model by running it through the past 125,000 years, including the last glacial cycle and Holocene, using proxy-data time series of temperature and sea level. The temperature time series, having a 50-year resolution and spanning 100,000 years, (Johnsen et al. 1995), is a reconstruction based on oxygen isotopes in the Greenland Ice-core Project (GRIP) ice core, which was taken in the vicinity of the ice-sheet summit.

The model runs are initiated 135,000 before present from a state that is in equilibrium with present-day conditions. During the Eem interglacial period, we assume 3°C higher temperatures than today for 125,000 years ago, which are linearly decreasing to –5.5°C colder than today

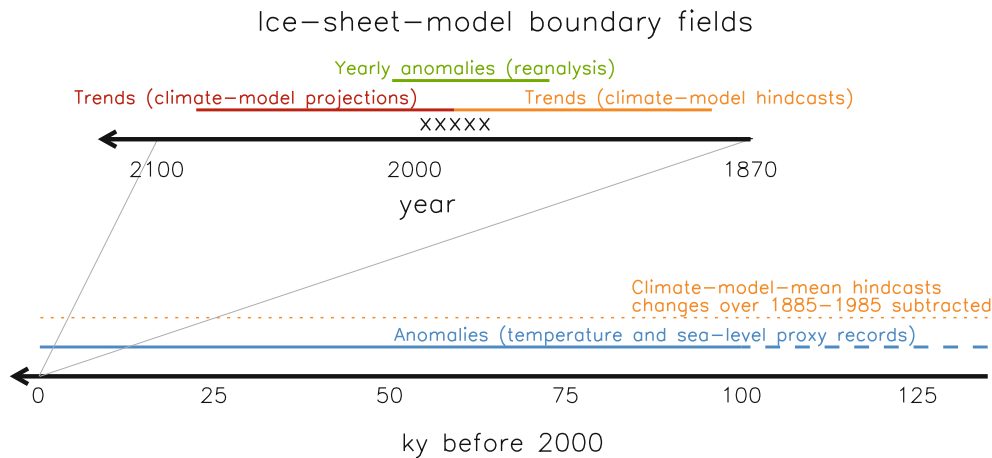


**Fig. 1** Boundary fields applied to the ice-sheet model. The  $x$ 's indicate the period over which the precipitation field and the parameterization of temperatures are estimated. All coloured lines indicate anomalies relative to this base period. The *solid, blue line* indicates temperature anomalies from the GRIP ice core (Johnson et al. 1995). The *dashed, blue line* covers the Eem interglacial period and the beginning of the latest glacial cycle. Here we assume that  $3^{\circ}$  higher temperatures than today are reached at around 125,000 years ago, which linearly decreased to  $-5.5^{\circ}$  relative to today at around 100,000 years ago, matching the onset of the GRIP record. The precipitation is scaled relative to the temperature anomalies (Clausen et al. 1988). A sea-level time series is applied back to 125,000 years ago (Imbrie et al. 1989). The *red line* indicates temperature and

precipitation trends from climate-model projections. In some runs these trends are substituted by yearly anomalies (see Sect. 5). The *solid, orange line* indicates trends from hindcasts by these models. The *dotted, orange line* indicates that the mean changes from the climate-model hindcasts are subtracted. This subtraction implies that the ice-sheet model reaches 19th-century, preindustrial conditions before the onset of the warming trends during the industrial time. The *green line* indicates detrended yearly anomalies of temperature and precipitation from the ERA-40 and ERA-Interim reanalysis data. These reanalysis anomalies were added during a model-evaluation experiment only. All fields are functions of latitude and longitude, except the temperature and sea-level data over the glacial cycle (*blue lines*)

for 100,000 years ago, matching the beginning of the GRIP record. The temperature development during the Eem has a negligible influence on today's ice-sheet distribution as given by the ice-sheet model, which we tested by setting the Eem maximum temperatures both  $3^{\circ}\text{C}$  warmer and colder than in the original experiment. Precipitation is given from the present-day precipitation, scaled by the annual-mean surface-temperature anomalies relative to today, following Clausen et al. (1988). We tested the Clausen et al. (1988) parameterization by comparing estimates using this method with precipitation changes given directly by the 100,000 year GRIP record. This comparison gives a root-mean-square difference between the two time series of less than 2%. The sea level during the past 125,000 years is taken from Imbrie et al. (1989).

### 2.2.2 Twentieth and twenty-first century evolution

In order to estimate the 21st century ice-sheet changes, the ice-sheet model is forced with precipitation and surface-air temperature changes estimated by the climate models listed in Table 1. These models were used for the IPCC Fourth Assessment Report and were included in the Coupled Model Intercomparison Project (CMIP3) archive (Meehl et al. 2007b). They represent the models with the highest performance score for the Northern Hemisphere extratropics in an evaluation by Gleckler et al. (2008). Many of

these models are also among the best performing models with regard to surface-air temperature and precipitation over Greenland as shown in evaluations by Franco et al. (2010) and Walsh et al. (2008).

Three fields from the climate models are used for the ice-sheet model: July-mean and annual-mean temperatures and annual precipitation. In order to estimate the uncertainty of the ice-sheet evolution due to the spread in projections among climate models, the ice-sheet models are run with fields from each of the climate models. As indicated in Table 1, some of these models have an ensemble of runs. In that case, the ensemble-mean field of the model in question is chosen.

In order to obtain the ice-sheet response to the full climate change as given by the climate models, from the preindustrial stage to the year 2100, hindcasts are used for the period 1870–2000 and projections thereafter. Hindcasts are estimated by including observed changes back to preindustrial time of forcing agents such as greenhouse gases and aerosols in the climate-model runs. For the future projections, the A2, A1B, and the B1 greenhouse-gas-emission scenarios are used (Nakićenović and Swart 2000), which represent a high, intermediate, and low scenario among those used for the AR4. The A1B scenario is based on the assumption of a rapid economical growth, an increase of the Earth population to 9 billion by 2050, and a globalised society implying, for instance, that new technology spreads easily around the world.

**Table 1** Climate models used for the sea-level change projections

CMIP3 name	Centre	Ensemble # hindcast (21st century)
CGCM3.1(T47)	Canadian Centre for Climate Modeling	5 (5)
CGCM3.1(T63)	Canadian Centre for Climate Modeling and Analysis (Canada)	1 (1)
CNRM-CM3	Météo France, Centre National de Recherches Météorologique (France)	1 (1)
GFDL-CM2.0	US Department of Commerce, NOAA de Recherches Météorologique (France)	3 (1)
GFDL-CM2.1	US Department of Commerce, NOAA Geophysical Fluid Dynamics Laboratory (USA)	3 (1)
ECHAM5	Max-Planck-Institut für Meteorologie (Germany)	4 (4)
CCSM3	National Center for Atmospheric research (USA)	5 (7)
UKMO-HadGEM1	Hadley Centre for Climate Prediction and Research, Met Office (UK)	2 (1)
UKMO-HadCM3	Hadley Centre for Climate Prediction and Research, Met Office (UK)	2 (1)
MRI-CGCM2.3.2	Meteorological Research Institute (Japan)	5 (5)
CSIRO-Mk3.0	CSIRO Atmospheric Research (Australia)	3 (1)
CSIRO-Mk3.5	CSIRO Atmospheric Research (Australia)	3 (1)
MIROC3.2-medium	CCSR/NIES/FRCGC (Japan)	3 (3)
MIROC3.2-hires	CCSR/NIES/FRCGC (Japan)	1 (1)

The last column gives the number of ensemble members for the hindcast runs and for 21st century runs, where the latter is indicated by parenthesis

Two sets of temperature and precipitation differences between three 30-year averages 1870–1899, 1970–1999, and 2070–2099, constitute the 20th and 21st century changes. The climate-model mean of these fields are shown in Fig. 2. These changes over the 20th and 21st century,  $\Delta X_{20}$  and  $\Delta X_{21}$ , are added to the preindustrial state,  $X_{pi}$ , of the ice-sheet model:

$$X(t) = \begin{cases} X_{pi}(t), & t < 1885, \\ X_{pi}(t) + \frac{t-1885}{100} \Delta X_{20}, & 1885 \leq t < 1985, \\ X_{pi}(t) + \Delta X_{20} + \frac{t-1985}{100} \Delta X_{21}, & 1985 \leq t < 2085, \\ X_{pi}(t) + \Delta X_{20} + \Delta X_{21}, & 2085 \leq t, \end{cases}$$

where  $X$  indicates July and annual-mean temperatures and annual-mean precipitation and  $t$  is time in years. All  $X$  fields are functions of horizontal space coordinates.

The development of the ice-sheet height may feedback on the 20th and 21st century temperature and precipitation changes, which is not taken into account by the climate models, since they all have constant topography of the ice sheets. We take this feedback into account by dividing the changes into a constant part and a part that for temperature depends on surface height, and for precipitation depends on the gradient of the surface height. This split is done by a linear regression of the temperature and precipitation changes on the surface height and the gradient of the surface height, respectively. For example for temperatures, the split of  $\Delta X_{20}^T$  into these two parts gives:

$$\Delta X_{20}^T(t) = R_{20}^T h(t) + \delta X_{20}^T,$$

where  $R_{20}^T$  is a regression coefficient:

$$R_{20}^T = \left[ \int h^o(t_0) h^o(t_0) dA \right]^{-1} \int \Delta X_{20}^T(t_0) h^o(t_0) dA,$$

and  $\delta X_{20}^T$  is the residual which can be found from:

$$\delta X_{20}^T = \Delta X_{20}^T(t_0) - R_{20}^T h^o(t_0).$$

The surface height is denoted by  $h(t)$ ,  $h^o(t_0)$  is present-day surface height as given by observations (Bamber et al. 2001), and  $A$  denotes the ice-sheet area. Precipitation changes are regressed on the gradient of the surface height rather than the surface height itself.

The basic state of the surface temperature and precipitation of the ice-sheet models is based on observations during recent decades. We therefore first subtract in the beginning of the ice-sheet-model runs the climate-model-mean 20th-century changes. Hereby the models arrive at preindustrial conditions around 1870, before the onset of the changes over the industrial period.

In order to evaluate the ice-sheet model, the present-day surface height and mass balance, as simulated by the model, are compared with observations. For that reason a special experiment is undertaken, where detrended yearly anomalies of temperature and precipitation from reanalysis data over the period 1958–2008 are added. Hereby the model provides a more detailed picture of the surface-mass balance during recent decades. ERA-40 data are used until 1989 and ERA-Interim data (Simmons et al. 2008) thereafter. The reanalysis data were detrended by subtracting the linear trend so that only yearly anomalies were retained. Hence over the period 1958–2008 both 20th-century changes from the climate-models and reanalysis anomalies

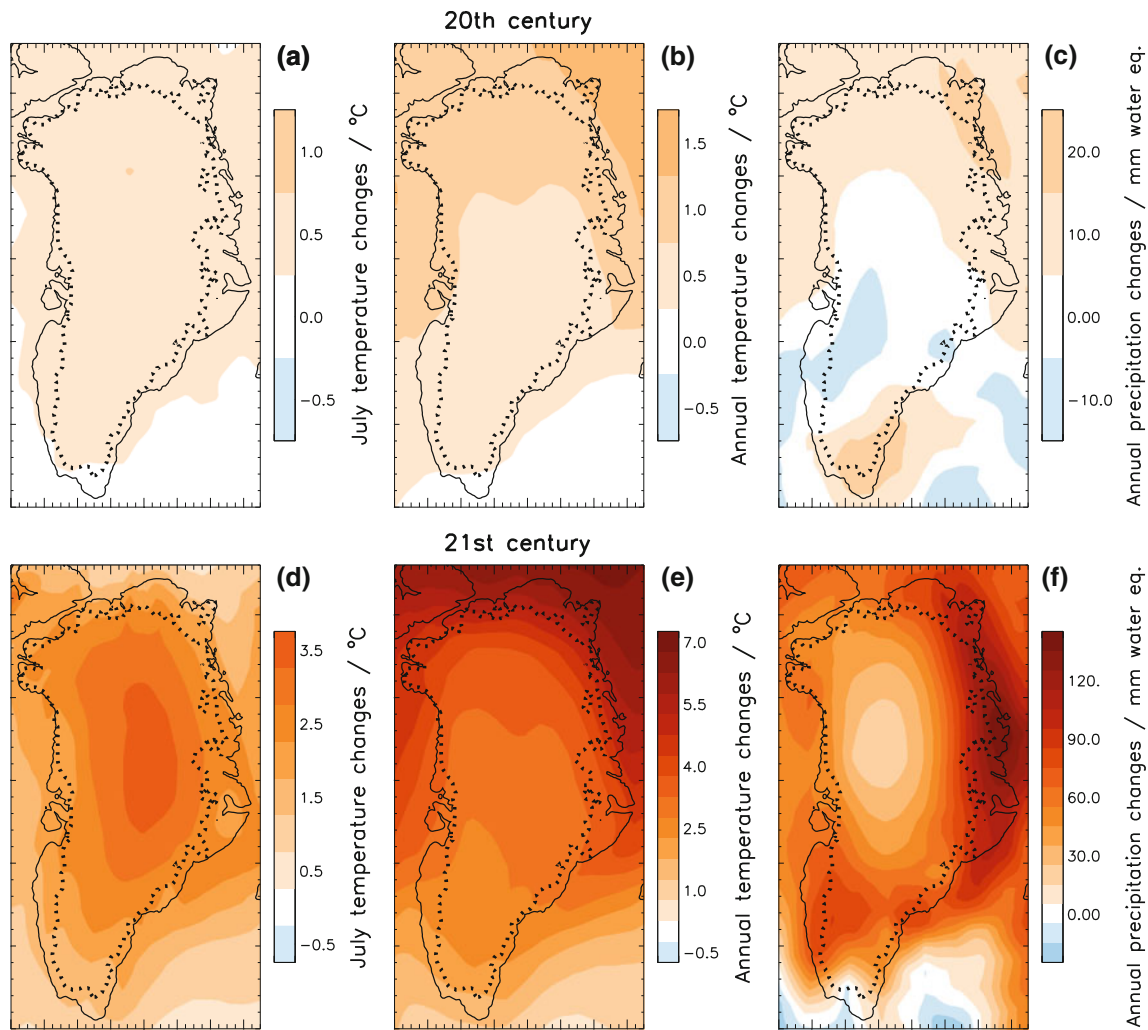


**Fig. 2** Climate-model-mean temperature and precipitation changes over Greenland during 1885–1985 (*upper panels*) and 1985–2085 (*lower panels*). **a** and **d** show July temperature changes, **b** and **e** annual-mean temperature changes, and **c** and **f** show annual

precipitation changes. *Solid and dotted, black lines* indicate the observed present-day coast line and ice edge, respectively, as given by Bamber et al. (2001)

are added to the model during this evaluation experiment. Here the climate-model mean is used for the 20th-century changes.

### 2.3 Outlet glaciers and model tuning

When the ice reaches fjords, it may float on the water. For floating ice the bottom friction is negligible. The ice motion at the ice-sheet edge is opposed by a normal stress due to the water pressure and shear stresses exerted by the side walls of the fjords (Paterson 1994). The spatial variations of such stresses may also constitute the dominating forces for other outlet glaciers that are not floating, but sliding over the ground. These stresses are not taken into account by the zero-order shallow-ice approximation normally used for the ice-sheet model. In addition, the width of the outlet glaciers is often smaller than a few kilometers

and is therefore not resolved on the grid of today's ice-sheet models.

In an attempt to include the effect of these fjords, the sliding is enhanced by implementing a sliding enhancement factor which is set to higher values in the vicinity of the fjords (Fig. 3). This implementation provides a major contribution to the model tuning. Hence, the magnitude of the sliding enhancement for each fjord is chosen so that the model reproduces the present-day surface height relative to observations as close as possible. As the ice retreats, the enhancement can propagate inland as long as the bedrock is below sea-level. Such conditions apply for the Jakobshavn Isbræ and for areas in the northeast and northwest of Greenland. The fjords are localized on the basis of the bedrock topography provided by Bamber et al. (2001). Since the scales of the fjords are often smaller than the 10 x 10 km model resolution, their positions in the model

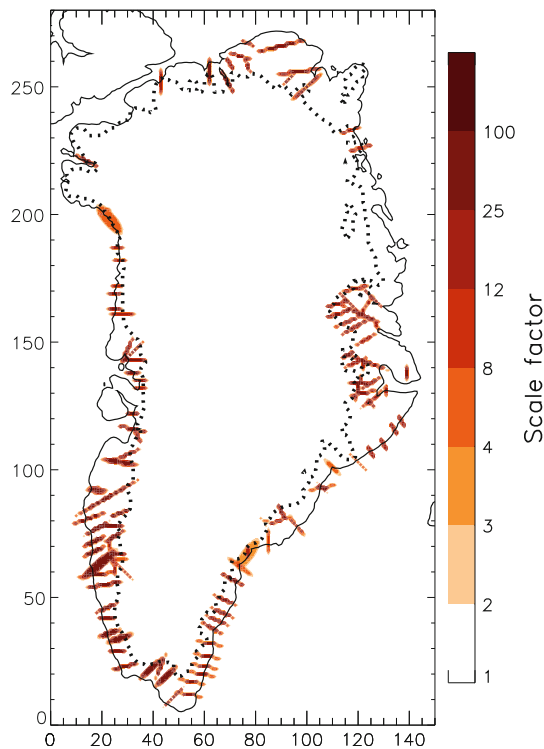


**Fig. 3** Factor used for increasing the sliding in the vicinities of fjords. The present-day coast line and the ice edge are indicated as in Fig. 2

do not exactly agree with their real positions. The enhancement factor for a given fjord is kept about constant along the fjord using a hyperbolic tangent function with an elliptic shape, which approximates the shape of the fjord.

The implementation of a sliding enhancement factor also provides the possibility to take into account an observed general increase of the outlet-glacier flow during recent years (Joughin et al. 2004; Rignot et al. 2008; Howat et al. 2008). During the last glacial period and the Holocene, the sliding enhancement is kept fixed to the values indicated in Fig. 3. From 1990 and onwards it is further enhanced in order to simulate the observed increase in the dynamical discharge.

We emphasize that we do not aim to present an improved ice-dynamical model, which implicitly solves the problem of correctly representing the flow of the outlet glaciers. Rather we implement a pragmatic parameterization which captures the major aspects of this flow.

The model is tuned as to reduce the bias between model and observations of the present-day surface height. As mentioned above, the sliding enhancement in the vicinity of outlet glaciers is used for tuning. In addition, the settings of an ice-flow enhancement factor in the dynamical model, and the standard deviation of daily temperature variability in the mass-balance model are used for tuning. The flow enhancement factor, which is associated with plastic ice

deformation, is set to 1.75 at the ice-sheet surface increasing to 3.7 at the bottom, following the vertical variations given by Mangeney and Califano (1998). These variations take the change of anisotropy with height into account as mentioned above.

The standard deviation of daily and diurnal variability of temperature, which is used for estimating a positive degree-day potential in the mass-balance model, is normally set around 5°C (Huybrechts and de Wolde 1999). We set it to 5.2°C in the north of Greenland linearly increasing to 6°C in the south. This increase towards lower latitudes is qualitatively consistent with a latitudinal variation of the diurnal cycle of incoming solar radiation during summer when melting is important.

The settings of these tuning parameters—including those for the outlet-glacier enhancement—are chosen so that the model represents fairly well the present-day ice-sheet height and its discharge as shown in Sects. 3 and 4. This may not represent the ultimate tuning minimizing the biases. However, such a perfect tuning is not necessary here, since we explore the ice-sheet model uncertainty when it comes to the 21st century sea-level-rise projections.

#### 2.4 Estimation of uncertainty due to ice-sheet-model settings

The ice-sheet-model uncertainty is estimated by varying parameters and boundary fields that are not fully determined. This is done in two steps: First, experiments are performed where a single model parameter is set to (or a field is scaled with) what we judge as being extreme values, both in the high and the low end as indicated in Table 2. Second, experiments with combinations of these settings, which during the first step resulted in the most extreme responses in terms of 21st-century mass loss, are performed. The boundary fields are perturbed by applying a scaling factor.

Some of the models that are constructed by perturbations of parameters and boundary fields produce unrealistic present-day ice sheets. We disregard such models if their present-day ice-sheet volume deviates by more than 30% of the observed value which is 2.9 million km<sup>3</sup> (Bamber et al. 2001). For the tuned model, the present-day ice-sheet volume is ~3.2 million km<sup>3</sup> which is about 10% larger than observed.

We regard the 30% present-day ice-sheet-volume limit and the ranges of the parameters and boundary-field scaling factors (Table 2) as extreme choices. As a consequence, the ice-sheet model ensemble for exploring uncertainty includes models with rather extreme parameter and scaling settings. This implies that the resulting range of uncertainty is an upper-bound estimate.

**Table 2** Parameters that are varied in order to explore ice-sheet model uncertainty

Name	Description	Setting	Range of exploration
Dynamical model:			
Enh	Flow enhancement factor for plastic deformation flow	See Sect. 2.1.1	50–150%
Slid	Sliding coefficient	$1.8 \times 10^{-10} \text{ N}^{-3} \text{ year}^{-1} \text{ m}^7$	25–200%
OutGlac	Increase of sliding parameter in the vicinity of outlet glaciers	See Sect. 2.3	0–200%
GeoThm	Geothermal heat flux	$1.33 \times 10^6 \text{ J m}^{-2} \text{ year}^{-1}$	80–150%
Mass-balance model:			
TMA	Annual mean temperature	Parameterization	$\pm 2^\circ\text{C}$
TMJ	July mean temperature	Parameterization	$\pm 2^\circ\text{C}$
Tstd	Standard deviation of daily temperature variability	$5^\circ\text{C}$	80–120%
PDDs	Snow melt factor of PDD	0.003 m water eq. per degree day	90–110%
PDDi	Ice-melt factor of PDD	0.007 m water eq. per degree day	90–110%
ReFree	Freeze of snow-melt water and rain	See Sect. 2.1.2	No freeze, freeze during summer
Lithosphere model:			
TauBd	Relaxation time scale for bed rock	3,000 years	1,500–7,000 years
Boundary fields:			
Prec	Precipitation	See Sect. 2.1.2	$\pm 20\%$
TGRIP	Last glacial period and Holocene temperatures	See Sect. 2.2.1	$\pm 20\%$

### 3 Outlet-glaciers

The inclusion of the simple parameterization of outlet-glaciers flow (Sect. 2.3), provides a more realistic estimate of the present-day surface height of the ice sheet. This is evident from Fig. 4, which shows the difference between ice-sheet height from model and observations, both when the effects of the fjords are taken into account and when they are ignored. Both ice-sheet models are run over the past 125,000 years. From 1870 and onwards the climate-model-mean precipitation and temperature trends are added.

The inclusion of the parameterization of outlet glaciers results in considerable improvements along the ice-sheet edge, especially in the northern and south-western part. The root-mean-square ice-sheet-height difference between the model and observations is  $\sim 195$  m when the effects of fjords are included, but reaches  $\sim 275$  m when they are ignored. In the northern part, deep fjords are present in an area that is not covered by the ice sheet today. In the model, the ice sheet builds up over this area during the previous glacial period. During the Holocene, the ice sheet does not retreat to the present-day state if the effect of the fjords is not included in the model.

Many outlet glaciers attain more realistic velocities in the model when the sliding is enhanced in the vicinity of fjords. Figure 5 shows modeled and observed velocities along the Jakobshavn Isbræ as a function of distance from the ice edge in the observations. Without the sliding enhancement of this outlet glacier, the velocities are considerable smaller than when the enhancement is included. In the latter case, the velocities show a spatial structure that is more comparable to the observations, although the observations still show larger magnitudes, and a position of the ice edge further inland relative to the model. The observations are from the period around 2000–2008 (Joughin et al. 2010). They are therefore from the end of a decade when speed up and retrieval of this outlet glacier has been observed (Joughin et al. 2004). A comparison between model and observation of maximum velocities at some of the major outlet glaciers is given in Table 3.

### 4 Mass balance during recent years

In the previous section and in Fig. 4a it was shown that the present-day surface height from a model, which includes

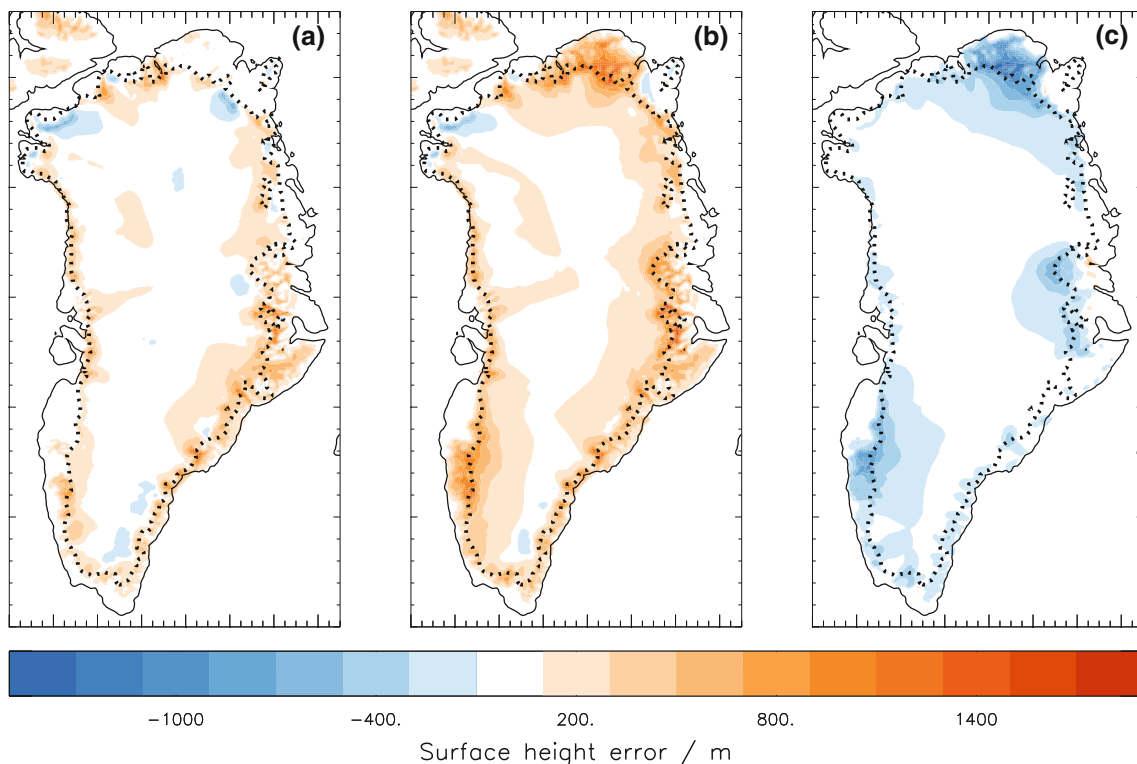


**Fig. 4** Bias of the present-day (year 2000) modeled surface height relative to the observations given by Bamber et al. (2001), when a sliding enhancement factor in the vicinity of the outlet glaciers is

included (a) and not included (b). The difference between (a) and (b) is given by (c). The present-day coast line and the ice edge are indicated as in Fig. 2

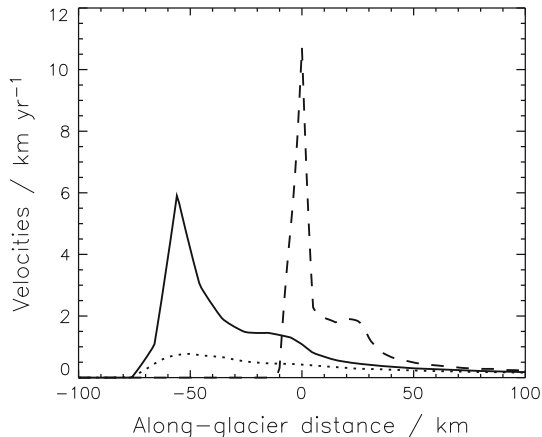


**Fig. 5** Maximum velocities along Jakobshavn Isbræ diagonal to the ice edge. Zero distance is set at the point of maximum velocity in the observations, and positive distances are upstream. The solid and dotted lines are for a model including and ignoring, respectively, enhancement of outlet-glacier sliding. The dashed line is for observations which are taken as a mean over measurements from January 2000, June 2005, July 2006, and September 2008 (Joughin et al. 2010)

enhanced sliding of outlet glaciers, compares reasonable well with observations, and it performs better than the standard ice-sheet model. In this section, the modeled total mass-balance during the last decades is compared with observations. Again, the ice-sheet model is run over the

**Table 3** Maximum velocities of selected outlet glacier, from observations and models with and without enhanced outlet-glacier sliding

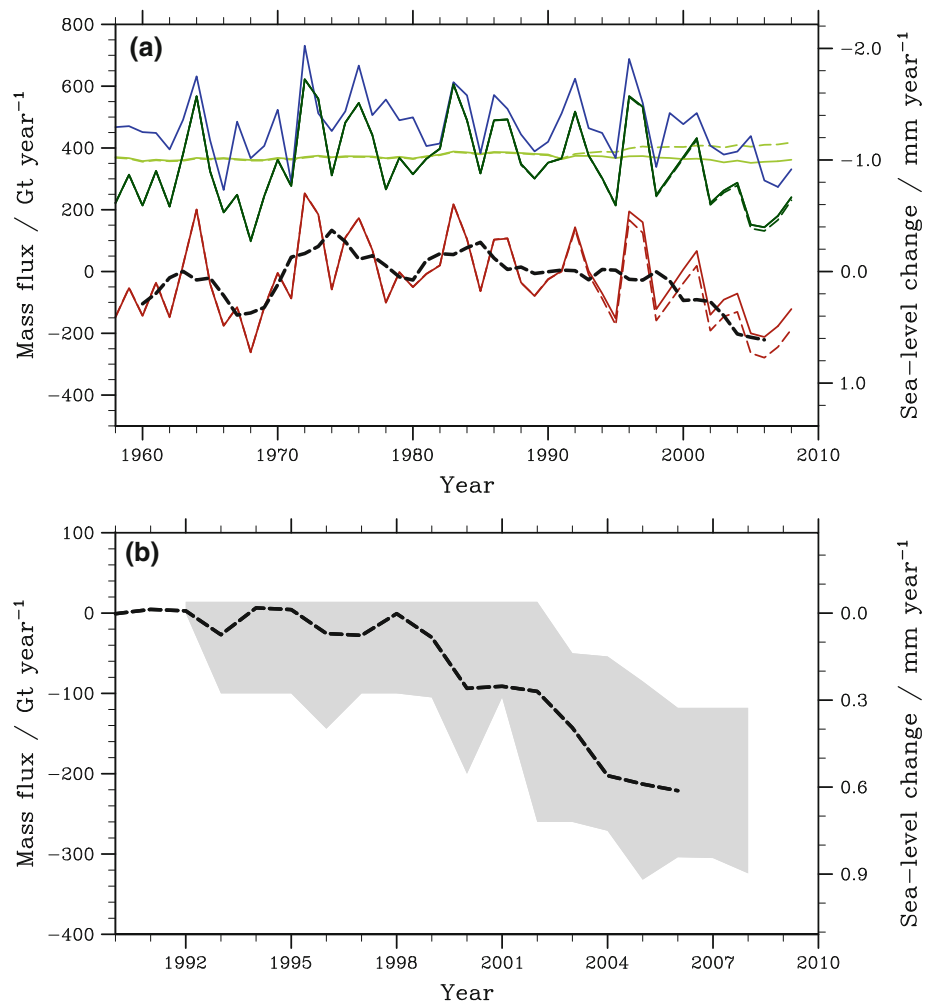
	Observations	Enhanced sliding	No enhanced sliding
<i>Jakobshavn Isbræ</i>	6 <sup>†</sup> ; 10.7 <sup>+</sup>	6.0	2.2
<i>Kangerdlugssuaq</i>	7.3*; 6.3 <sup>+</sup>	7.5	6.8
<i>Helheim</i>	8.4*	7.1	2.9
<i>Ikeq</i>	4*; 12.3 <sup>+</sup>	5.0	3.7

Observations are from (†) Joughin et al. 2004, from the beginning of the 1990s; (\*) Howat et al. 2008, from around year 2000; and (⁺) Joughin et al. 2010, from 2000–2008. Units are in km year<sup>-1</sup>

past 125,000 years. From 1870 and onwards the climate-model-mean surface-air-temperature and precipitation trends are added.

The modeled surface-mass balance (SMB), which is the difference between accumulation and runoff and integrated over the ice sheet, is given by the dark-green, solid line in Fig. 6 for 1958–2008. Over this period, yearly anomalies of temperature and precipitation are taken into account (Sect. 2.2.2). A corresponding SMB estimate from an energy-balance model implemented in the RACMO regional climate model (RCM) is shown by the blue line (van den Broeke et al. 2009; Ettema et al. 2009). These two estimations of the SMB are not entirely independent, since the present-day

**Fig. 6** Mass balance of the Greenland ice sheet over the period 1958–2010. In **a**, *dark-green lines* indicate the surface-mass balance, SMB, the *light-green lines* the dynamical discharge,  $D$ , the *red lines* the total mass balance, SMB-D, while the *black line* gives a 5-year running-mean estimate of SMB-D. The *dashed lines* are for a model with increased sliding of outlet glaciers beginning in 1990, and the *solid lines* are for a model without sliding increase. The *blue line* indicates SMB as estimated by van den Broeke et al. (2009). In **b**, the 5-year running mean of SMB-D (*dashed line*) is given along with the observations and their uncertainties (*gray shading*). The observations are from Katsman et al. (2010)



precipitation field used for the ice-sheet model is estimated by the same RCM simulation. However, in the RCM, the SMB is calculated on the basis of the observed present-day ice-sheet topography, whereas in the ice-sheet model, the topography has freely evolved over the last glacial period and the Holocene. In addition, for the ice-sheet model, the SMB is estimated on the basis of a PDD approach, whereas an energy-balance model is used within this RCM.

The year-to-year variability of two SMB estimates agree fairly well, though the time-mean SMB for the ice-sheet model, 348 Gt year<sup>-1</sup>, is smaller than that from the RCM, 466 Gt year<sup>-1</sup>, but is in agreement with the value given by Rignot et al. (2008),  $\sim 340$  Gt year<sup>-1</sup>. The latter is a combination of two different PDD-model-based results (Box et al. 2006; Hanna et al. 2008). Also the variability in terms of the standard deviation is larger for the ice-sheet model, 129 Gt year<sup>-1</sup>, than for the RCM, 103 Gt year<sup>-1</sup>. This may indicate that the PDD-model is more sensitive to temperature and precipitation forcing than is the energy-balance model, which is in accordance with earlier results (Van de Wal and Oerlemans 1994; van de Wal 1996; Bougamont et al. 2007).

Dynamical discharge,  $D$ , is given by the light-green, solid line in Fig. 6a. As mentioned in Sect. 2.3, the flow of many outlet glaciers has increased during the last two decades. In total this has led to an increase of the dynamical discharge by 10–20% between 1996 and 2008 (van den Broeke et al. 2009, their Fig. S3 which is based on results from Rignot et al. 2008). The implementation of the sliding enhancement factor allows for taking into account an increase of dynamical discharge. In order to mimic the observed increase, the sliding enhancement is gradually increased from 1990 in the vicinity of the outlet glaciers, so that the dynamical discharge increases by about 15%. The dashed, dark-green and light-green line give the SMB and  $D$  for this experiment. The total surface-mass balance, SMB-D, is indicated by the red lines. The black dashed line is a 5-year running mean of the SMB-D in the case of the sliding enhancement.

Observational estimates of the total mass balance during recent decades are indicated by the gray shading in Fig. 6b. This observational range includes all observations and their uncertainties as given by Katsman et al. (2010). Observations show that the rate of mass loss increased from  $\sim 0$  to 100 Gt year<sup>-1</sup> around 1995 to  $\sim 100$ –300 around 2005. A

comparison of the modeled total mass balance averaged over 5 years (Fig. 6b, black, dashed lines) and these observations indicates that the model results are within the range of uncertainty of the observations.

### 5 Greenland’s contribution to sea-level rise during the 21st century

In summary of the two previous sections, the ice-sheet model, with our settings of parameters, provides realistic results with respect to the total ice-sheet height and the evolution of the total mass balance over the last two decades. After this assessment of the current climate, the model is now run another 100 years ahead in order to estimate contributions to sea-level changes by the end of the 21st century. To this end, the model is forced with temperature and precipitation changes over the period from 1870 to 2100, taken from various climate-model runs (Sect. 2.2.2)

Projections of sea-level change, on the basis of temperature and precipitation trends from the ensemble of climate models forced by the A1B greenhouse-gas emission scenario, are shown by the coloured lines in Fig. 7. Due to the spread among climate models, future changes range from 1.9 to 8.0 cm, where the upper and lower bound are associated with the UKMO-HadGEM1 and the GFDL-CM2.1 trends, respectively. Without temperature and

precipitation forcing over the 21st century, the ice-sheet model estimates that the ice sheet is almost in balance, which is indicated by the black, dashed line.

The gray lines in Fig. 7 show all perturbation-ensemble members, which are ice-sheet models where model parameters and boundary fields have been perturbed (Sect. 2.4). The ice-sheet model uncertainty is explored using future predictions from both the UKMO-HadGEM1 and the GFDL-CM2.1 model, since these two models constitute the spread among climate models with regard to the melt response of the Greenland ice-sheet during the 21st century. Not all perturbation-ensemble members produce realistic present-day ice sheets. For example, the model that projects ~13 cm of sea-level rise by the year 2100 provides an ice volume in the year 2000 of only 1.2 million km<sup>3</sup> which is less than 50% of the observed value. This model was set with 2°C warmer July temperatures than the unperturbed version. We disregard this model since it deviates by more than 30% relative to the observed volume. In this case, we then construct a model with a more moderate perturbation of the July temperature for the perturbation ensemble.

The total uncertainty including spread among climate models, various greenhouse-gas emission scenarios, as well as the ice-sheet model uncertainty is given in Fig. 8a. Dark-green shading indicates the spread among climate models for the A1B emission scenario. The red and blue shading is model spread for the A2 and B1 scenario,

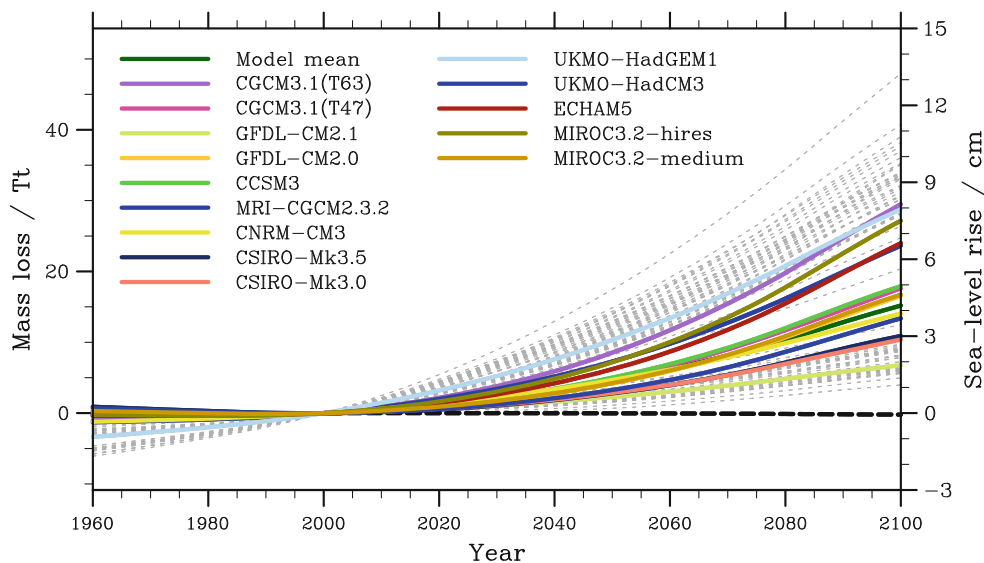


**Fig. 7** Projections of Greenland’s contribution to sea-level rise for the 21st century. Projections are based on the ice-sheet-volume anomalies relative to the year 2000 assuming an ice density of 910 Kg m<sup>-3</sup> and an Earth ocean area of 36.2 million km<sup>2</sup>. Left axis gives the ice-sheet-mass change in 10<sup>12</sup> ton, whereas the right axis provides the associated total sea-level rise. The *coloured lines* show projections using temperature and precipitation trends over the 20th and 21st century from the climate models indicated in the frame. These climate models are forced with the A1B emission scenario of greenhouse

gases. *Gray lines* show all perturbation runs, where parameters and boundary fields have been perturbed in the ice-sheet model as outlined in Sect. 2.4. These perturbation runs are all based on trends from the UKMO-HadGEM1 and the GFDL-CM2.1 model, since these models represent the spread among climate models with regard to the 21st century Greenland ice-sheet change. *Black, dashed line* indicates projections when no 21st-century forcing is applied to the ice-sheet model

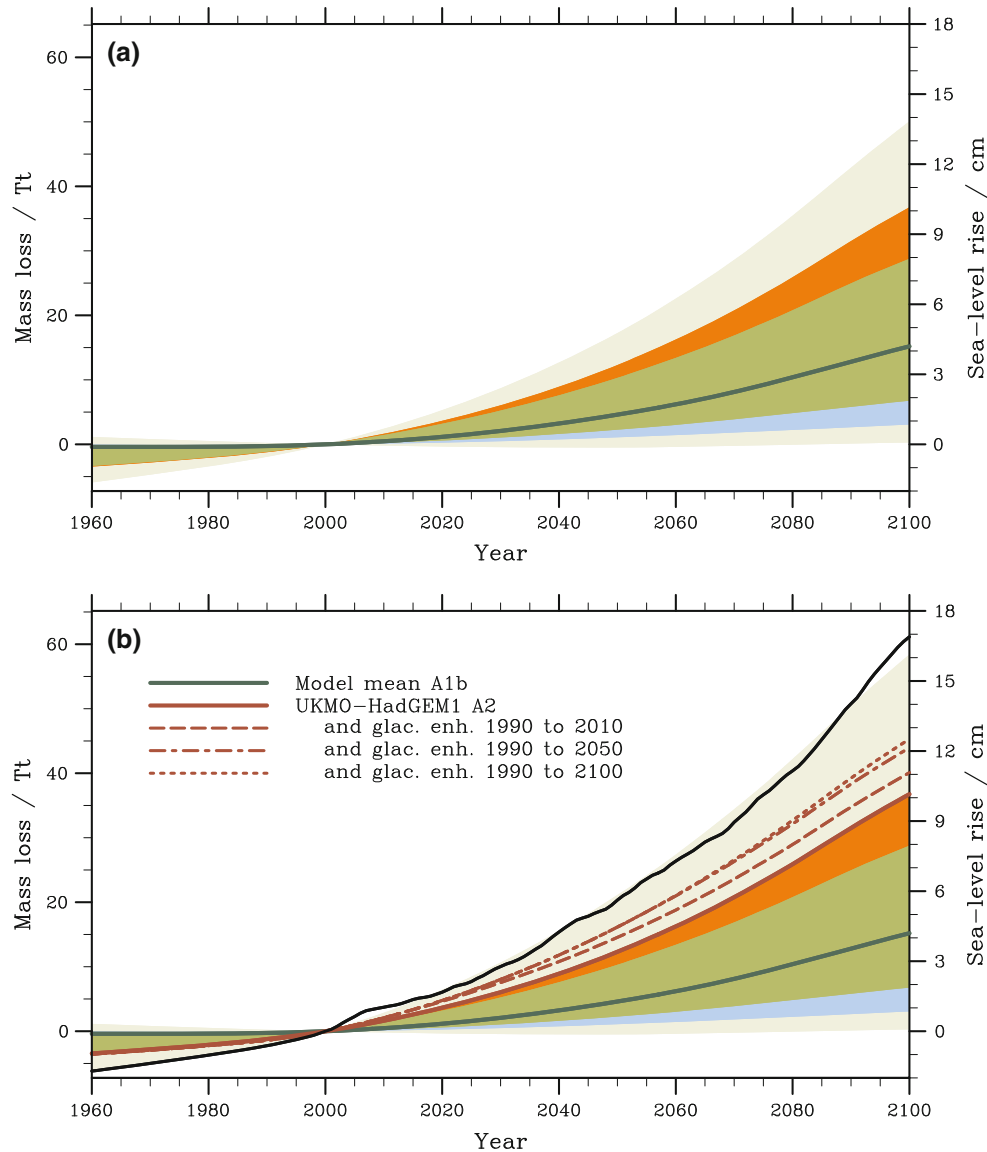


**Fig. 8** Sea-level-rise projections for the 21st century. The *dark, green shading* indicates the spread among climate models for the A1B greenhouse-gas emission scenario. The *red shading* shows the spread among climate models for the A2 scenario, which is not intersecting the spread for the A1B scenario. The *blue shading* indicates a corresponding spread for the B1 scenario. The *light-green shading* shows additional spread due to ice-sheet-model uncertainty. This is based on the ensemble of perturbation runs, as indicated in Fig. 7, excluding runs that resulted in unrealistic ice sheets (see Sect. 5 for details). In **b**, the *red lines* indicate runs with trends from the UKMO-HadGEM1 model forced with the A2 scenario. The *red, solid line* indicates a run without enhancement of outlet-glacier sliding, whereas runs including enhanced sliding, over periods indicated in the frame,

are given by the other *red lines*. In **a**, the *light-green shading* spans the uncertainties of the ice-sheet model with UKMO-HadGEM1 A2-scenario trends, and the model based on the GFDL-CM2.1 B1-scenario trends. In **b**, the *light-green shading* spans uncertainty as in **a** except that enhancement of outlet-glacier sliding during 1990–2100 is included in the ice-sheet model with UKMO-HadGEM1 A2-scenario trends. The *black line* shows the projection by this latter ice-sheet model where the UKMO-HadGEM1 A2-scenario trends are substituted by the yearly anomalies over the 21st century. The UKMO-HadGEM1 had only one ensemble member for the A2 scenario. This model run gives the highest sea-level-rise projection among all experiments. The vertical axes are as in Fig. 7

respectively, which is not intersected by the spread from the A1B scenario. Finally, the light-green shading indicates the additional range due to uncertainty of the ice-sheet model and its boundary fields.

A further source of uncertainty is the future behavior of the outlet glaciers. As mentioned in Sect. 4, the model can

reproduce the observed increase in dynamical discharge when gradually increasing a sliding enhancement factor in the vicinity of outlet glaciers. We now add this gradually increase of sliding to the model that is based on the UKMO-HadGEM1 trends. Red lines in Fig. 8b show projections for three different periods of sliding increase:

1990–2010, 1990–2050, 1990–2100. For example for 1990–2010, the sliding enhancement factor is gradually increased from 1990 to 2010 and then kept constant. The sliding enhancement over 1990–2010 gives  $\sim 0.9$  cm of additional sea-level rise by 2100, whereas over 1990–2050 and 1990–2100 gives  $\sim 2.0$  and 2.4 cm, respectively. Apparently, the response in terms of sea-level rise saturates when the enhancement factor is increasing over a successively longer period. This is so, because the dynamical discharge depends on the ice-sheet height and its gradient in the vicinity of the outlet glaciers. The ice velocities are dependent on the gradient of the surface height, and the amount of discharge is dependent on both the velocities and the ice thickness. When the outlet-glacier flow increases due to the sliding enhancement, it may reduce both the ice-sheet height and its gradient. Hence this constitutes a negative feedback process that damps the dynamical-discharge increase induced by the enhancement of the sliding.

In order to take all uncertainties into account, we add the UKMO-HadGEM1 trends and the entire 21st-century sliding increase in the models of the perturbation ensemble used for exploring the ice-sheet-model uncertainties. Light-green shading in Fig. 8b gives the range of uncertainty when all four sources of uncertainty are taken into account: climate model spread, greenhouse-gas emission scenarios, outlet glaciers speed up, and the uncertainty of the ice-sheet model and its boundary conditions.

For simplicity, linear trends of surface-air temperature and precipitation are used to estimate the sea-level-change projections mentioned above. Climate models exhibit natural variability on yearly and decadal time scales. Such variability in future climate-model scenarios of temperature and precipitation will likely be unpredictable and is therefore not taken into account for these sea-level-change projections. By using linear trends, the effect of this inter-annual variability is omitted. However, interaction between the ice sheet and the short-term variability of the precipitation and temperature forcing fields is likely non-linear. For instance, the ice-sheet may lose more mass in a warm year than it gains in a cold year, even though the warm and cold years are anomalies of the same magnitude (but opposite signs) relative to the linear trend. This effect is studied by running all ensemble members of each of the models using yearly anomalies of surface-air temperature and precipitation instead of the linear trends during the 21st century. The anomalies of temperature and precipitation are relative to the 1970–1999 average.

Two examples are given in Fig. 9a, b for the CCSM3 and the MRI-CGCM2.3.2 model. The runs with yearly variability from each ensemble member all indicate a larger sea-level change than the run with the linear trend based on the ensemble mean. In order to estimate the non-linear effect

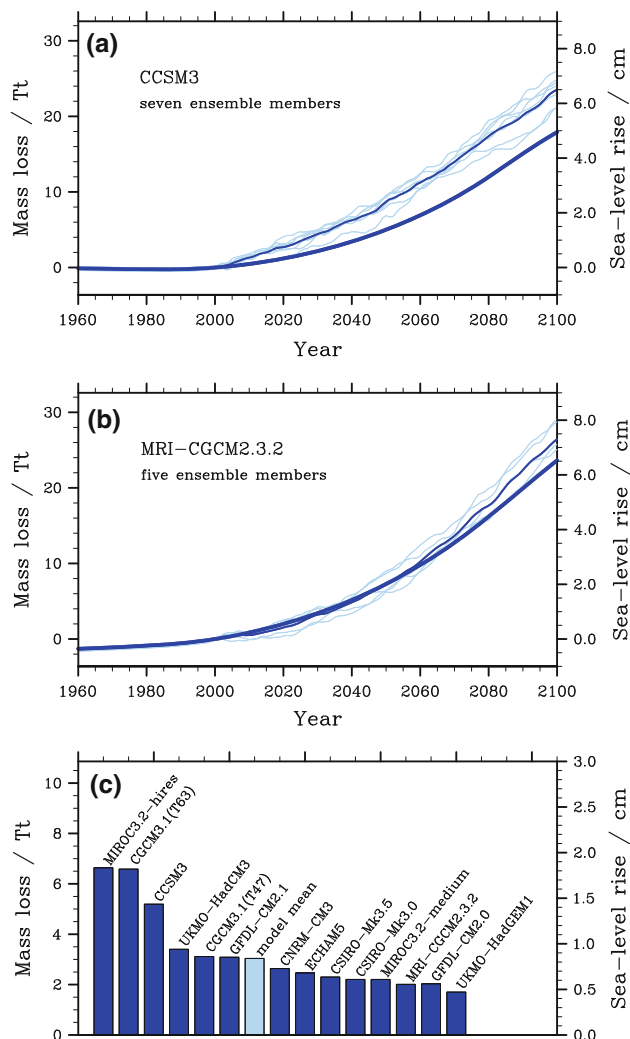


**Fig. 9** Comparison of projections based on linear trends and yearly anomalies of surface-air temperatures and precipitation from climate models over the 21st century. As an example, **a** and **b** show for the CCSM3 and the MRI-CGCM2.3.2 model projections based on yearly anomalies for each ensemble member (*light-blue lines*), their mean (*thin, dark-blue line*), and based on the linear trend (*thick, dark-blue line*). **c** indicates difference between the mean of the ensemble-member projections based on yearly variability and the projection based on the linear trend (the *dark-blue lines* in **a** and **b**). The difference is averaged over 2071–2100. The results are presented for each model (*dark-blue bars*) and the model mean (*light-blue bar*). The vertical axes are as in Fig. 7

associated with the inter-annual variability, the difference between the mean of the ensemble runs and the run with the linear trend is calculated. Figure 9c provides differences for each of the models where the differences are averaged over 2071–2100. The effects associated with the inter-annual variability of temperature and precipitation are positive for all models and give up to 2 cm of additional sea-level rise by the end of the 21st century.

Finally we explore whether this non-linear effect could extend the upper limit of the sea-level change, which was

given above on the basis of the linear trends. In the ice-sheet model that gives the most extreme response in terms of sea-level change (this is the model providing the upper edge of the light-green shading in Fig. 8b) the linear trends of temperature and precipitation are now substituted with yearly anomalies. These forcing fields are from the UKMO-HadCM1 model for the A2 scenario which has only 1 ensemble member. The black line in Fig. 8b shows the resulting sea-level-change projection which adds about 1 cm to the upper estimate based on the linear trends.

## 6 Discussion and conclusions

We estimate that the Greenland ice sheet will contribute  $\sim 0$ –17 cm to sea-level rise by the end of the 21st century. Our methods for the estimation of this range of uncertainty go beyond those used for the AR4 by, for instance, implementing a parameterization for outlet-glacier speed up and adding future changes of temperature and precipitation directly to ice-sheet models. Table 4 presents the split of the uncertainty range into its components. The major part of the uncertainty is due to the spread among climate models, which is followed by the contribution from the ice-sheet models.

Outlet glacier speed up stands for up to  $\sim 2.5$  cm of sea-level change by the end of the 21st century (Table 4). The AR4 projects a value of  $1 \pm 0.5$  cm based on extrapolation of dynamical discharge during 1993–2003. This value can be compared with our scenario of enhanced outlet-glaciers sliding during 1990–2010, which likewise gives a contribution of 1 cm (Fig. 8b). However, when the outlet-glacier sliding continues to increase throughout the 21st century, the sea-level-rise response becomes no more than 2.5 cm. This is smaller than the maximum contribution from what is mentioned as scaled-up ice-sheet discharge projected by the AR4. For the three greenhouse-gas emission scenarios that we consider, the AR4 projects a maximum of 13 cm

from both ice sheets where around a third of this ( $\sim 4$  cm) can be attributed to Greenland.

The sea-level rise of 17 cm is found to be an upper bound estimate, which can only be reached for a certain combination of parameter settings and scaling of the boundary field of the ice-sheet model. As mentioned in Sect. 4, the SMB from our model over the last five decades shows larger annual variability than that estimated with the energy-balance model implemented in an RCM (Van den Broeke et al. 2009). This energy-balance approach is more advanced than the PDD method used here, since, for instance, it takes solar radiation and albedo changes into account. Comparisons of PDD models and energy-balance models have shown that the former produce a larger runoff response than the latter for high temperatures (van de Wal 1996; Bougamont et al. 2007). Although experiments with perturbations of several PDD-model parameters are included in the perturbation ensemble for estimating the ice-sheet-model uncertainty, the PDD model, due to its simplicity, may still overestimate future runoff, irrespectively of its parameter settings. However, the shortcomings of the PDD model are unlikely to influence the upper bound estimate found here.

Vermeer and Rahmstorf (2009) find on the basis of a simple model, which relates total sea-level to global-mean temperature, that the AR4 underestimates the sea-level rise over the coming 100 years by at least a factor of two. The melt from the Greenland ice-sheet constitutes an important part of the total sea-level rise during the next 100 years. For the three greenhouse-gas emission scenarios that we consider, the AR4 reports a range of 1–8 cm due to SMB changes and 0–2 cm associated with dynamical-discharge changes. This gives a maximum of 10 cm of sea-level rise. Though our results indicate a higher upper bound estimate than that from the AR4, we cannot confirm that the AR4 underestimates with a factor of two when it comes to the Greenland contribution.

**Acknowledgments** The authors are thankful to Wouter Greuell, Frank Selten, Caroline Katsman, Bert Wouters as well as two anonymous reviewers for useful comments on the manuscript. The authors would like to acknowledge Janneke Ettema for providing RACMO precipitation data, Michiel van den Broeke for RACMO mass-balance data, and Bo Vinther for providing the GRIP ice-core data. R. Graversen is funded by Ministry of Transport, Public Works and Water Management, The Netherlands, within the project Abrupt Climate Scenarios.

**Table 4** Uncertainty of Greenland's sea-level-rise contribution by the end of the 21st century as given from Fig. 8

Total	Scenario	Climate model	Ice-sheet model	Outlet-glacier speed up
16.1	3.2	6.1	4.4	2.4

The scenario uncertainty is based on the A2, A1B, and B1 greenhouse-gas emission scenario. The climate model uncertainty is estimated on the basis of the models in Table 1. The ice-sheet model uncertainty is based on an ensemble of models, constructed on the basis of the settings indicated in Table 2. This includes uncertainty of, for instance, the mass-balance model and the dynamical ice-flow model except for the uncertainty associated with outlet-glacier speed up. The latter is given separately. Units are in cm

## References

- Bueler E, Brown J (2009) Shallow shelf approximation as a “sliding law” in a thermodynamically coupled ice sheet model. *J Geophys Res* 114. doi:10.1029/2008JF001179
- Bamber JL, Layberry RL, Gogineni SP (2001) A new ice thickness and bed data set for the Greenland ice sheet 1. Measurement, data reduction, and errors. *J Geophys Res* 106:33,773–33,780

- Bintanja R, van de Wal RSW, Oerlemans J (2002) Global ice volume variations through the last glacial cycle simulated by a 3-D ice-dynamical model. *Quat Int* 95–96:11–23
- Bintanja R, van de Wal RSW, Oerlemans J (2005) Modelled atmospheric temperatures and global sea levels over the past million years. *Nature* 437:125–128
- Bintanja R, van de Wal RSW (2008) North American ice-sheet dynamics and the onset of 100,000-year glacial cycles. *Nature* 454:869–872
- Box JE, Bromwich DH, Vennhuis BA, Bai, L-S, Stroeve JC, Rogers JC, Steffen K, Haran T, Wang S-H (2006) Greenland Ice Sheet Surface Mass Balance Variability (1988–2004) from Calibrated Polar MM5 Output. *J Clim* 19:2783–2800
- Bougamont M, Bamber JL, Ridley JF, Gladstone RM, Greuell W, Hanna E, Payne AJ, Rutt I (2007) Impact of model physics on estimating the surface mass balance of the Greenland ice sheet. *Geophys Res Lett.* doi:10.1029/2007/GL030700
- Clausen HB, Gundestrup NS, Johnsen SJ, Bindschadler R, Zwally J (1988) Glaciological investigations in the Crête area, Central Greenland. A search for a new deep-drilling site. *Ann Glaciol* 10:10–15
- Ettema J, van den Broeke MR, van Meijgaard E, van de Berg WJ, Bamber JL, Box JE, Bales RC (2009) Higher surface mass balance of the Greenland ice sheet revealed by high-resolution climate modeling. *Geophys Res Lett.* doi:10.1029/2009GL038110
- Franco B, Fettweis X, Erpicum M, Nicolay S (2010) Present and future climate of the Greenland ice sheet according to the IPCC AR4 models. *Clim Dyn.* doi:10.1007/s00382-010-0779-1
- Gleckler PJ, Taylor KE, and Doutriaux C (2008) Performance metrics for climate models. *J Geophys Res* 113. doi:10.1029/2007JD008972
- Gregory JM, Huybrechts P (2006) Ice-sheet contributions to future sea-level change. *Phil Trans R Soc A* 364:1709–1731
- Hanna E, Huybrechts P, Steffen K, Cappelen J, Huff R, Shuman C, Irvine-Fynn T, Wise S, Griffiths M (2008) Increased runoff from melt from the Greenland ice sheet: a response to global warming. *J Clim* 21:331–341
- Hindmarsh RCA (2006) The role of membrane-like stresses in determining the stability and sensitivity of the Antarctic ice sheets: back pressure and grounding line motion. *Phil Trans R Soc A* 364:1733–1767
- Holland DM, Thomas RH, de Young B, Ribergaard MH, Lyberth B (2008) Acceleration of Jakobshavn Isbræ triggered by warm subsurface ocean waters. *Nat Geosci* 1:659–664
- Howat IM, Joughin I, Fahnestock M, Smith BE, Scambos TA (2008) Synchronous retreat and acceleration of southeast Greenland outlet glaciers 2000–06: ice dynamic and coupling to climate. *J Glaciol* 54:646–660
- Huybrechts P (1990) A 3-D model for the Antarctic ice sheet: a sensitivity study on the glacial-interglacial contrast. *Clim Dyn* 5:79–92
- Huybrechts P, de Wolde J (1999) The dynamical response of the Greenland and Antarctic ice sheets to multiple-century climate warming. *J Clim* 12:2169–2188
- Imbrie JD, McIntire A, Alan C (1989) Ocean response to orbital forcing in the late Quaternary: observational and experimental strategies. In: Berger A, Schneider SH, Duplessy JC (eds) *Climate and geosciences, a challenge for science and society in the 21st century*. Kluwer, Boston, pp 121–164
- Johnsen SJ, Dahl-Jensen D, Dansgaard W, Gundestrup N (1995) Greenland paleotemperatures derived from GRIP bore hole temperature and ice core isotope profiles. *Tellus* 47B:624–629
- Joughin I, Abdalati W, and Fahnestock M (2004) Large fluctuations in speed on Greenland's Jakobshavn Isbræ glacier. *Nature* 432:608–610
- Joughin I, Smith BE, Howat IM, Sambos TA (2010) Greenland flow variability from ice-sheet-wide velocity mapping. *J Glac* 56:415–430
- Katsman CA, Sterl A, Beersma JJ, van den Brink HW, Church JA, Hazeleger W, Kopp RE, Kroon D, Kwadijk J, Lammersen R, Lowe J, Oppenheimer M, Plag H-P, Ridley J, von Storch H, Vaughan DG, Vellinga P, Vermeersen LLA, van de Wal RSW, Weisse R (2010) Exploring high-end scenarios for local sea level rise to develop flood protection strategies for a low-lying delta. *Clim Change* (Submitted)
- Lythe MB, Vaughan DG (2001) BEDMAN: a new ice thickness and subglacial topographic model of Antarctica. *J Geophys Res* 106:11,335–11,351
- Meehl GA, Stocker TF, Collins WD, Fiedlingstein P, Gaye AT, Gregory JM, Kitoh A, Knutti R, Murphy JM, Noda A, Raper SCB, Watterson IG, Weaver AJ, Zhao Z-C (2007a) Global climate projections. In: Solomon S, Qin D, Manning M, Chen Z, Marquis M, Averyt KB, Tignor M, Miller HL (eds) *Climate change 2007: the physical science basis. Contribution of Working Group I to the Fourth Assessment Report of the International Panel on Climate Change*, Cambridge University Press, Cambridge, New York
- Meehl GA, Covey C, Delworth T, Latif M, McAvaney B, Mitchell JFB, Stouffer RJ, Taylor KE (2007b) The WCRP CMIP3 multimodel dataset, a new era in climate change research. *Am Meteorol Soc.* doi:10.1175/BAMS-88-9-1383
- Mangeney A, Califano F (1998) The shallow ice approximation for anisotropic ice: formulation and limits. *J Geophys Res* 103:691–705
- Nakićenović N, Swart R (2000) *Emission scenarios*. Cambridge University Press, UK
- Ohmura A (1987) New temperature distribution maps for Greenland. *Zeitschrift für Gletscherkunde und Glazialgeologie* 23:1–45
- Paterson WSB (1994) *The physics of glaciers*, 3rd edn. Butterworth-Heinemann, Oxford
- Pfeffer WT, Meier MF, Illangasekare TH (1991) Retention of Greenland runoff by refreezing: implication for projected future sea level change. *J Geophys Res* 96:22,117–22,124
- Reeh N (1991) Parameterization of melt rate and surface temperature on the Greenland ice sheet. *Polarforschung* 59:113–128
- Rignot E, Box JE, Burgess E, Hanna E (2008) Mass balance of the Greenland ice sheet from 1958 to 2007. *Geophys Res Lett.* doi:10.1029/2008GL035417
- Simmons A, Uppala S, Dee D, Kobayashi S (2006) ERA-Interim: new ECMWF reanalysis products from 1989 onwards. *ECMWF Newsl* 110:25–35
- Straneo F, Hamilton GS, Sutherland DA, Stearns LA, Davidson F, Hammill MO, Stenson GB, Rosing-Asvid A (2010) Rapid circulation of warm subtropical waters in a major glacial fjord in East Greenland. *Nat Geosci* 3:182–186
- Van de Berg J, van de Wal RSW, Milne GA, Oerlemans J (2008) Effect of isostasy on dynamical ice sheet modelling: a case study for Eurasia. *J Geophys Res* 113. doi:10.1029/2007JB004994
- Van den Broeke M, Bamber J, Ettema J, Rignot E, Schrama E, van de Berg WJ, van Meijgaard E, Velicogna I, Wouters B (2009) Partitioning recent Greenland mass loss. *Sci* 326:984–986
- Uppala SM, Kållberg PW, Simmons AJ, Andrae U, Bechtold V da C, Florino M, Gibson JK, Haseler J, Hernandez A, Kelly GA, Li X, Onogi K, Saarinen S, Sokka N, Allan RP, Andersson E, Arpe K, Balmaseda MA, Beljaars ACM, van de Berg L, Bidlot J, Bormann N, Caires S, Chevallier F, Dethof A, Dragosavac M, Fisher M, Fuentes M, Hagemann S, Hólm E, Hoskins BJ, Isaksen I, Janssen PAEM, Jenne R, McNally AP, Mahfouf J-F, Morcrette J-J, Rayner NA, Saunders RW, Simon P, Sterl A, Trenberth KE, Untch A, Vasiljevic D, Viterbo P, Woollen J

- (2005) The ERA-40 re-analysis. *Q J R Meteorol Soc* 131:2961–3012
- Walsh JE, Chapman WL, Romanovsky V, Christensen JH, Stendel M (2008) Global Climate Model Performance over Alaska and Greenland. *J Clim* 21:6156–6174
- Van de Wal RSW (1996) Mass-balance modelling of the Greenland ice sheet: a comparison of an energy-balance and a degree-day model. *Ann Glac* 23:36–45
- Van de Wal RSW (1999a) The importance of thermodynamics for modeling the volume of the Greenland ice sheet. *J Geophys Res* 104:3887–3898
- Van de Wal RSW (1999b) Processes of buildup and retreat of the Greenland ice sheet. *J Geophys Res* 104:3899–3906
- Van de Wal RSW, Oerlemans J (1994) An energy balance model for the Greenland ice sheet. *Glob Plan Change* 9:115–131
- Vermeer M, Rahmstorf S (2009) Global sea level linked to global temperature. *PNAS*. doi:[10.1073/pnas.0907765106](https://doi.org/10.1073/pnas.0907765106)